A conditional disaggregation algorithm for generating fine time-scale rainfall data in a warmer climate

by:

Seth Westra[1], Jason Evans[2], Rajeshwar Mehrotra[3], and Ashish Sharma[3]

[1] School of Civil, Environmental and Mining Engineering

University of Adelaide, Adelaide, Australia 5005

Email: seth.westra@adelaide.edu.au

Tel: +61 8 8313 1538, Fax: +61 8 8303 4359

[2]Climate Change Research Centre, Faculty of Science,

University of New South Wales, Sydney, Australia 2052

[3] School of Civil and Environmental Engineering,

University of New South Wales, Sydney, Australia, 2052

Keywords: Downscaling, disaggregation, sub-daily rainfall, extreme rainfall, temperature scaling, generalized additive model, method of fragments

Abstract

This paper describes an algorithm for disaggregating daily rainfall into sub-daily rainfall 'fragments' (fine-resolution rainfall sequences) under a future, warmer climate. The algorithm uses a combined Generalised Additive Model (GAM) and Method of Fragments (MoF) framework to resample sub-daily rainfall fragments from the historical record conditional on daily rainfall amount and a range of atmospheric covariates. The rationale is that as the atmosphere warms, future rainfall patterns will be more reflective of historical rainfall patterns corresponding to warmer days at the same location, or to locations which have an atmospheric profile more reflective of expected future climate.

It was found that the daily to sub-daily scaling relationship varied significantly by season and by location, with rainfall patterns on warmer seasons or at warmer locations typically showing more intense rainfall occurring over shorter periods compared with cooler seasons and stations. Importantly, by regressing against atmospheric covariates such as temperature, this effect was substantially reduced, suggesting that the approach may also be valid when extrapolating to a future climate. The GAM-MoF algorithm was then applied to nine stations around Australia, with the results showing that relative to the daily rainfall amount, the maximum intensity of short duration rainfall increased by between 4.1% and 13.4% per degree change in temperature for the maximum six minute burst, and by between 3.1% and 6.8% for the maximum one hour burst. The fraction of each wet day with no rainfall also increased by between 1.5% and 3.5%. This highlights that a significant proportion of the change to the distribution of rainfall is likely to occur at sub-daily timescales, with important implications for many hydrological systems.

39 ## 1. Introduction

40 Understanding likely changes to rainfall patterns resulting from anthropogenic emissions of greenhouse
41 gases remains an important and continuing area of research, both for scientific reasons to better constrain
42 expected changes to the global hydrological cycle, and due to the immense societal implications of any shift
43 in rainfall intensity or frequency [*Bates et al.*, 2008; *IPCC*, 2011]. Much of this research has focused on daily
44 or longer-scale precipitation changes, due in large part to the availability of high-quality global land-surface
45 precipitation datasets [*Gleason et al.*, 2002; *Klein Tank et al.*, 2002; *Peterson et al.*, 1997] to facilitate
46 research on historical precipitation changes [e.g. *Alexander et al.*, 2006; *IPCC*, 2011]. Furthermore, there is
47 now widespread availability of daily global climate model output as part of the CMIP3 and CMIP5 archives,
48 which have been used to understand possible future changes to rainfall as the atmosphere continues to
49 warm [*Allan and Soden*, 2008; *Allan et al.*, 2010; *Trenberth*, 2011].

50 Despite this, it is recognised that many of the physical processes of rainfall operate at much finer timescales,
51 and that changes at the finest timescales may not be properly captured by daily total rainfall amounts. For
52 example, it is well known that the evolution of individual convective systems occurs over timescales of
53 hours or less, with these systems often being responsible for the highest-intensity rainfall [*Wallace and*
54 *Hobbs*, 2006]. Furthermore, although rainfall is almost always caused by the upward motion of air
55 [*Trenberth et al.*, 2003], the mechanisms which drive this upward motion are diverse and vary significantly
56 over the course of a single day [*Evans and Westra*, 2012], with no *a priori* reason for suggesting that each of
57 these mechanisms would change in the same manner in a future climate.

58 One important line of evidence in this area concerns investigations into the scaling relationship between
59 rainfall and temperature, using historical sub-daily rainfall and atmospheric temperature data in Europe,
60 Australia and Japan [*Berg et al.*, 2009; *Haerter et al.*, 2010; *Hardwick-Jones et al.*, 2010; *Lenderink and van*
61 *Meijgaard*, 2008; *Lenderink et al.*, 2011; *Utsumi et al.*, 2011]. The basic hypothesis being tested by all these
62 studies is that extreme rainfall will scale at a rate proportional to the moisture holding capacity of the
63 atmosphere, which increases by about 7% per degree as governed by the Clausius-Clapeyron (C-C)

relationship [*Trenberth*, 2011; *Trenberth et al.*, 2003]. The general conclusions of these and other studies suggest that the true scaling relationship is much more complex than is implied by this simple thermodynamic relationship, however, with research showing that the scaling is affected by:

(1) the extremity (or recurrence interval) of the rainfall event, with more extreme rainfall typically exhibiting greater scaling with temperature compared with less extreme events;

(2) the duration of the rainfall event, with hourly or sub-hourly rainfall bursts exhibiting higher scaling compared with daily rainfall;

(3) the atmospheric temperature, with Lenderink and van Meijgaard [2008] finding C-C scaling at temperatures below 12°C, and double C-C scaling at greater temperatures in The Netherlands, whereas Hardwick-Jones *et al*. [2010] showed negative scaling at temperatures above about 26°C in Australia; and

(4) access to atmospheric moisture, with Hardwick-Jones *et al.* [2010] suggesting the decline above 26°C was likely to be attributed to insufficient moisture availability at these temperatures.

Furthermore Berg *et al.* [2009; *Haerter and Berg*, 2009] and Haerter and Berg [2009] hypothesise that rather than being driven purely by thermodynamic constraints, the change in rainfall intensity with temperature might be due to changes in rainfall type, shifting from large-scale synoptic systems in winter through to localised convective activity in summer.

Despite all this complexity, a consistent result between these studies is that the scaling between near-surface atmospheric temperature and sub-hourly rainfall appears to be much greater than for daily rainfall, highlighting that many of the expected changes in the future might also occur at these shorter timescales. In particular, different scaling rates at different timescales would result in a shift in the temporal distribution of rainfall, from lower-intensity rainfall occurring over longer periods throughout the day to higher-intensity rainfall occurring over shorter period [*Trenberth*, 2011], even under the hypothetical situation in which daily total rainfall remains constant.

88 Although the presence of a scaling relationship in the historical data does not necessary imply such changes
89 will continue into the future, several preliminary analyses of extreme rainfall trends during the late 20th and
90 early 21st centuries also show much stronger increases at hourly or sub-hourly timescales compared with
91 daily timescales [*Jakob et al.*, 2011; *Lenderink et al.*, 2011; *Westra and Sisson*, 2011]. Dynamical modelling of
92 changes to short-duration rainfall extremes has been limited due to the difficulties in resolving the physical
93 processes associated with convection, although two recent studies using cloud resolving models show
94 increases in line with the C-C rate [*Muller et al.*, 2011; *Romps*, 2011]. It should be noted, however, that
95 results from both these studies are based on an idealised situation over an increased sea surface
96 temperature field, and thus may not reflect changes to continental areas with limited moisture availability
97 such as in Australia.

98 In this paper we propose a statistical downscaling algorithm which is capable of yielding continuous rainfall
99 sequences down to the resolution of the observational network (6 minutes in the case of the Australian
100 example described here). The final algorithm aims to combine daily downscaling outputs which can be
101 generated using a range of downscaling techniques [e.g. *Charles et al.*, 1999a; *Charles et al.*, 1999b; *Fowler*
102 *et al.*, 2007; *Mehrotra and Sharma*, 2006; *Mehrotra and Sharma*, 2007; *Semenov and Barrow*, 1997;
103 *Semenov and Stratonovitch*, 2010] with a daily to sub-daily rainfall disaggregation algorithm that accounts
104 for changes in future rainfall patterns. As daily downscaling of precipitation is by now a reasonably mature
105 field and since the proposed algorithm can be coupled with a large variety of statistical and/or dynamical
106 daily downscaling algorithms, this paper describes the disaggregation component only.

107 The remainder of this paper is structured as follows. In the following section we describe the data used for
108 the study, including both the observational sub-daily rainfall record as well as the atmospheric predictors
109 used for defining 'atmospheric state'. In **Section 3**, we present the algorithm used for understanding the
110 daily to sub-daily rainfall scaling, commencing with the Generalised Additive Model approach for identifying
111 'similar' days of record in terms of atmospheric state, followed by a description of the Method of Fragments
112 algorithm which is used to re-sample historical rain days which have a similar atmospheric state compared
113 to what might be expected in the future. Section 4 then contains the results, including several analyses

directed at evaluating the capacity of the model to provide plausible projections of future sub-daily rainfall, as well as a sensitivity study to describe the likely changes to sub-daily rainfall as the atmosphere warms. Finally, a discussion and conclusions are provided in **Section 5**.

2. Data

2.1. Sub-daily Rainfall

The continuous sub-daily rainfall data used for this study was obtained from the Australian Bureau of Meteorology (www.bom.gov.au), which maintains digitised records of sub-daily rainfall gauges throughout Australia at resolutions of 6 minutes. For this study we focus on a subset of nine gauges from this larger record, with each of these gauges having near-continuous records over the period from 1979 through to 2006. This period has been selected to ensure consistency with the reanalysis data described later.

The gauge locations are summarised in **Table 1** and **Figure 1**, and these stations represent a wide range of climate zones, ranging from a tropical climate in the northern parts of Australia (and in particular Cairns and Darwin), through to mid-latitude and higher latitude climates further south. The diversity of climates can be seen when looking at the seasonal cycle of precipitation amounts and intensity, shown in **Figure 2**. Both in terms of rainfall amounts and intensity per wet day, the two tropical stations of Darwin and Cairns are clearly summer-dominated, with the majority of rainfall occurring in the summer half year from approximately November through to April. Brisbane, which is the third-most northerly station, is also summer dominated although proportionally more rain falls in the winter months compared with the more northerly stations. In contrast, Perth and Adelaide have climates which are winter dominated, with most of the rain falling during the period from May through to October. Interestingly, the seasonal cycle of rainfall intensity per wet day is less pronounced, particularly for Adelaide. Both regions derive most of their rainfall from mid-latitude storm tracks during these winter months, with the summer usually dominated by drier northerly air masses. Finally, the remaining stations do not show a strong seasonal cycle, although the total intensity per wet day declines progressively with latitude from Sydney through to Hobart.

2.2. Atmospheric predictors

At each gauge location, a range of atmospheric variables were extracted using the NCEP Climate Forecast

System Reanalysis (CFSR) product, which is detailed at length in Saha *et al* [2010]. The data is available from 1979 to present, at a grid spacing of 0.5° x 0.5° longitude and latitude. The data was downloaded at an hourly temporal resolution, and was originally produced through a combination of short forecasts (the guess field), modified by assimilating new observations every six hours.

The increased spatial and temporal resolution of this new reanalysis product allows for the extraction of information at sub-daily timescales which might be useful for understanding the relationship between daily and sub-daily rainfall. The variables selected for analysis are summarised in **Table 2**, and include various variables measuring temperature at 2m above the land surface as well as three levels in the atmosphere, a number of variables reflecting moisture availability in the atmosphere (relative humidity and dew point depression), mean sea level pressure, and variables reflecting wind strength and direction. These variables include the predictor variables used by Beuchat *et al*. [2011] together with a range of additional variables commonly used in statistical downscaling [*Fowler et al.*, 2007]. These variables embody both the thermodynamics and dynamics of the lower atmosphere, and hence provide information on processes that may trigger and/or sustain precipitation. Furthermore, these variables have been used successfully in past applications [see *Mehrotra and Sharma*, 2010] and exhibit a reasonable level of consistency across GCMs in future climate simulations [*Johnson and Sharma*, 2009].

3. Methodology

3.1. Overview of the GAM-MoF algorithm

This paper describes a new Generalised Additive Model – Method of Fragments (GAM-MoF) technique for simulating the full temporal distribution of sub-daily rainfall conditional on daily rainfall amount and a set of atmospheric covariates described in **Table 2**. The algorithm can be viewed as an 'analogues' technique in which days in the historical record are sampled with an atmospheric state that is identified as being 'similar' to a projected future atmospheric state. A schematic of the algorithm is shown in **Figure 3**, and comprises the following four steps:

166 **Step 1:** Using historical sub-daily data, a number of metrics are defined which describe the daily to sub-daily
167 scaling behaviour for each day of record. We use the same metrics that were identified in Westra *et al*.
168 [2012], and which comprise the fraction of daily rainfall occurring in the maximum six minute and one hour
169 storm bursts (calculated by dividing the depth of rainfall occurring in the most intense six minute or
170 contiguous one hour storm bursts by the total daily rainfall depth for that day), as well as the fraction of the
171 day with no rainfall (calculated by counting the number of six minute increments with no rainfall and
172 dividing by the total number of six minute increments; i.e. 240). These scaling metrics were selected as part of
173 the development of a daily to sub-daily rainfall disaggregation algorithm described in Westra et al.[2012] based
174 on the finding that they captured a large part of the information on the scaling relationship between daily and
175 fine time-scale rainfall, and the reader is referred to that paper for more information. Only wet days are
176 considered in the analysis, and are defined based on a threshold of 1mm, with the study by Westra *et al*.
177 [2012] showing limited sensitivity to this threshold.

178 **Step 2:** A GAM was fitted between daily rainfall and various other atmospheric covariates described in **Table**
179 **2** as the predictor variables, and the daily to sub-daily scaling metrics identified in Step 1 as the response.
180 The GAM is used to identify the atmospheric covariates which have the greatest influence on the sub-daily
181 temporal pattern, and more details on the GAM methodology is provided in **Section 3.2**.

182 **Step 3:** Having trained and tested the GAM using historical data, it is possible to apply the model using
183 atmospheric covariates which are representative of a future climate. In this study we only provide a
184 sensitivity analysis in which we change atmospheric temperature while holding the remaining atmospheric
185 variables constant, however it is conceptually straight forward to couple the algorithm to a variety of
186 dynamical or statistical models which provide information on future rainfall at the daily timescale. Such an
187 algorithm provides information on the scaling metrics directly, but will not provide information on the full
188 temporal distribution of rainfall.

189 **Step 4:** To derive the full sub-daily rainfall temporal pattern, the final step is to use the MoF logic to identify
190 days in the historical record which have a 'similar' atmospheric state to those projected to occur in the
191 future, and sample the historical temporal pattern from one of those days. This is described further in

192 **Section 3.3**.

193 **3.2. Description of the GAM methodology**

194 A GAM-based modelling framework was adopted as it enables the simulation of linear and non-linear
195 relationships between the predictor and response variables together with variable interactions, and is
196 capable of simulating factor variables as well as continuous variables as part of the same modelling
197 framework.

198 Generalised additive models were first developed by [*Hastie and Tibshirani*, 1986; 1990], and a textbook
199 length treatment is provided in Wood [2006]. The latter reference was used as the basis for the analysis of
200 this paper, and the R software package [www.r-project.org] *mgcv* was used for the implementation of the
201 GAM. The benefits of GAMs are that they provide a flexible modelling structure which allows the response
202 variable to depend on a sum of smooth functions of predictor variables, while also allowing the distribution
203 of the response variable to be represented by any distribution from the exponential family. The general
204 expression for a GAM is given as [*Wood*, 2006]:

205 $$g(\mu) = \mathbf{X}^*\boldsymbol{\theta} + f_1(x_1) + f_2(x_2) + f_3(x_{3,}x_{4,})$$

206 where

207 $\mu = \mathbb{E}(\mathrm{Y})$, and Y ~ an exponential family distribution

208 Here **X*** represents the model matrix of parametric components, **θ** is the parameter vector, and the f_j are
209 smooth functions of covariates x. Thus this modelling framework allows for the simulation of linear
210 components as well as smooth functions, and by specifying smoothing functions in more than one
211 dimension such as $f_3(x_3, x_4)$ in the equation above, interactions between covariates can be simulated. Factor
212 variables, in which the variables are grouped into different levels such as by rainfall gauge location, can also
213 be accommodated into the model by using dummy indicator variables within the linear component of the
214 model.

215 The GAM framework provides some important advantages for the application proposed in this paper. For
216 example, one of the response variables (the six minute burst) has a highly skewed distribution, with a lower
217 bound of 1/240 = 0.00417 and an upper bound of 1. The application of a logarithmic transform to this data
218 yields an approximately Gaussian distribution. Likewise when considering the predictor variables, we wish
219 to model factor variables (e.g. individual stations), continuously distributed variables (e.g. sea level
220 pressure), lower bounded variables (e.g. daily total rainfall, wind strength), lower and upper bounded
221 variables (e.g. relative humidity), while potentially also considering the interactions between them.
222 Furthermore, the relationship between predictor and response may or may not be linear; for example using
223 the day of the year as a predictor variable to model seasonality of each of the response variables, the days
224 at the beginning and end of the year are likely to be more similar to those days in the middle of the year.
225 Specific issues related to the formulation of individual variables are described where relevant in later
226 sections of this paper.

227 The significant advantages in flexibility are tempered somewhat by the difficulty in model selection. This can
228 relate to the choice of smoothing function, the decision on which predictor variables to retain, and other
229 aspects of model selection such as the specification of the probability distribution or link function, each of
230 which can have some bearing on the predictions derived from the model. The results in this paper address
231 this issue in two ways: firstly through inspection of various diagnostic plots summarised in more detail
232 below to ensure that the modelling assumptions are met; and secondly through trialling a range of different
233 predictor selection methods and smoothing functions and evaluating whether the general conclusions
234 described in this paper are sensitive to specific model setup.

235 Following the suggestion of Wood [2006], for most of this paper we use tensor product smoothing functions
236 as the basis for estimating the smooths in one or more dimensions. The reason for this selection is that
237 most other smooths assume isotropy of the 'wiggliness' penalty (which determines how smooth the fitted
238 model becomes), which means that wiggliness in all dimensions is treated the same and thus does not
239 account for the potentially different properties of each of the covariates. In particular, a limitation of the
240 isotropic assumption for the present study is that many of the variables are in different units and represent

241 different quantities (e.g. atmospheric temperature and daily total rainfall), so that treating the wiggliness
242 penalty the same in all dimensions does not have any physical justification.

243 For predictor selection we have applied a ridge penalty to the smoothing term, which means that the term
244 can be shrunk to zero (i.e. the smooth returns to a linear model). The benefit is that the model strongly
245 penalises complexity, such that non-linear terms are not introduced without sufficient support from the
246 data. Finally, smoothing parameters are estimated automatically using a generalised cross-validation
247 criterion to prevent over-fitting of the smooths.

248 A range of diagnostics was used to evaluate the fit of the model, including quantile-quantile plots, residuals
249 vs. linear predictor, and response vs. fitted values. These diagnostics are not shown in this paper due to the
250 large number of plots, but were checked for all the fitted models described below using the framework
251 recommended by Wood [2006]. In the case of the fraction of rainfall in the maximum six minute storm burst
252 as the response variable, the best model was in fact a Gaussian model with an identity link function, but
253 applied to the natural logarithm of the response. A disadvantage of this structure is that the response
254 variable and all the associated diagnostics are now available as a non-linear function of the variable of
255 interest. Only a slight deterioration (in terms of a slightly non-linear q-q plot) was noted when using the
256 original (untransformed) response with a Gamma model and log link function. This choice was therefore
257 used for most of the remainder of this paper.

258 In all the analyses described in Section 4, the sensitivity of the model results to the choice of GAM setup
259 was evaluated, including using the log-transformed maximum six minute storm burst as described in the
260 previous paragraph, as well as different choices of smooths. The sensitivity was generally found to be low,
261 and although changes to the absolute values of some of the results were sometimes noted, the primary
262 conclusions of this paper were robust to the modelling setup. Interestingly, as was also noted in Westra *et al.*
263 [2012], the modelling framework was robust to the metric used for daily to sub-daily scaling. In particular,
264 the results using the six minute rainfall burst were consistent with the those using the maximum one hour
265 rainfall burst, although the GAM diagnostics on this latter metric showed poorer model fits, due to the large

266 fraction of days with 100% of the daily rainfall falling within the maximum one hour burst (since the
267 probability that all the daily rainfall occurs within a storm burst increases as the length of that storm burst
268 increases). The results were also similar using the fraction of the day with no rainfall.

269 **3.3. Method of Fragments algorithm**

270 A limitation of the GAM framework is that each model only includes a single response variable, with most of
271 the analyses in this paper focusing on the fraction of rainfall occurring in the maximum six minute storm
272 burst. To derive the full temporal distribution of sub-daily rainfall, we couple this algorithm to a MoF
273 algorithm which was developed under historical climate assumptions by [*Mehrotra et al.*, 2012; *Westra et*
274 *al.*, 2012]. In the version presented here, the algorithm works by searching through the historical record for
275 days which have 'similar' or 'analogous' atmospheric states to what we might expect under a future climate
276 (e.g. similar temperature, relative humidity, and so on), and then re-samples the sub-daily rainfall patterns
277 from such a day.

278 The atmospheric covariates used are those derived using the GAM model, and as will be shown in Section 4,
279 these covariates are able to explain much of the daily to sub-daily rainfall scaling relationship. In this paper
280 we demonstrate the application of the algorithm via a sensitivity analysis in which we perturb the historical
281 atmospheric state by modifying the atmospheric temperature while holding other variables constant. We
282 focus on sampling sub-daily rainfall 'fragments' from the same location, however we note that it would be
283 straight forward to generalise the algorithm to also take fragments from physiographically 'nearby' stations,
284 or even stations which are more distant but considered to be climatologically analogous to the location of
285 interest under a future climate.

286 In the context of this sensitivity analysis, the algorithm uses the GAM framework described above as the
287 basis for re-sampling as follows:

288 (1) For all wet days in the historical record, store the values of each of the atmospheric covariates
289 based on the reanalysis data, and for each of these days use the fitted GAM to predict one of the
290 measures of daily to sub-daily scaling such as the fraction of daily rainfall occurring in the maximum

six minute burst.

(2) Say we wish to simulate a series with an increase of 1°C atmospheric temperature. Then for a given wet day of interest, use GAM to predict the daily to sub-daily measure using the atmospheric variables for that day, but with the temperature variables increased by 1°C.

(3) Using the predicted daily to sub-daily measure in step (2), rank all the days in step (1) by proximity to this measure. Then for a deterministic model select the 'fragment' from the lowest ranked day, or for a stochastic model select the low ranked days randomly, with the highest probability given to the lowest ranked station [see equation 2 in *Westra et al.*, 2012].

Ideally the result of this algorithm would reflect a day with atmospheric predictors that are identical to those of the day of interest, except that the atmospheric temperature would be 1°C warmer. Because of a finite historical record, it is unlikely that there will be a day on record with exactly the same atmospheric covariates as the day of interest. The use of the GAM-based framework above allows for a sensible evaluation of the trade-off between different covariates, depending on the comparative influence of each atmospheric covariate on the daily to sub-daily scaling. For example, if the fitted GAM gives a strong relationship between the daily to sub-daily scaling metric and temperature, but a weak relationship with, say, geopotential height, then the algorithm above would aim to find days with similar temperature but potentially different geopotential heights as a basis for sampling.

4. Results

4.1. Investigating the influence of atmospheric temperature on daily to sub-daily scaling metrics

As highlighted in the introduction, the influence of atmospheric temperature on the scaling relationship between daily and finer time-scale rainfall has been the focus of a significant recent research effort, and provides a natural starting point for this analysis. In particular the scaling relationship between atmospheric temperature and short-duration rainfall implies that our daily to sub-daily scaling metrics should scale in proportion to the near-surface temperature of the atmosphere [*Hardwick-Jones et al.*, 2010; *Lenderink and*

316 *van Meijgaard*, 2008; *Lenderink et al.*, 2011; *Utsumi et al.*, 2011], and thus we start by examining the
317 relationship to this covariate.

318 We commence by examining the impact of seasonality on three measures of daily to sub-daily scaling: the
319 fraction of daily total rainfall occurring in the maximum six minute and one hour storm bursts, and the
320 fraction of each wet day with no rainfall. The emphasis on the seasonal cycle of these response variables is
321 because if a relationship between the daily to sub-daily scaling and temperature does indeed exist, then it
322 should come through clearly as seasonal variability, particularly in the higher latitude regions in Australia
323 where temperature varies strongly by season.

324 To account for this seasonal relationship, each daily to sub-daily scaling measure was regressed against day
325 of year (i.e. the series from 1 to 365/366). The results are shown in **Figure 4** for all cases where the predictor
326 'day of year' was significant. The few stations where this predictor was not significant included Adelaide
327 across each of the daily to sub-daily scaling measures, and Melbourne and Hobart just for the fraction of
328 day with no rainfall. In the case of Adelaide, the lack of significance may be due to the very limited rainfall
329 occurring in the summer months, making it difficult to evaluate the effects of the seasonal cycle on the
330 scaling relationship. In the case of Melbourne and Hobart, it is less clear why the seasonal cycle could not
331 be detected. The seasonal cycle for the other measures (fraction of rain falling in the one hour storm burst
332 and fraction of day with no rainfall) also was less pronounced at these two stations compared with other
333 locations, indicating that the seasonal cycle at these locations has a generally lower influence on daily to
334 sub-daily scaling.

335 For all the stations where a statistically significant seasonal cycle could be detected (defined as the predictor
336 'day of year' having a p value of 0.05 or less, although in almost all cases $p << 0.01$), the seasonal cycle
337 typically progressed from a maximum in the summer months to a minimum in the winter months. The
338 relationships were not only statistically significant but also practically important, with many of the stations
339 showing seasonal variations of up to 50% or more from the seasonal minima to the seasonal maxima in
340 each of the metrics. The direction of change for each of the three measures was also consistent: during the

341 times of the year with warmer temperatures, the amount of rain falling as shorter and more intense storm
342 bursts increases, and this is accompanied by an increase in the length of dry periods. The exception to this
343 result was for Darwin, which had the maximum for each of the metrics in the winter months, however these
344 results should be viewed in light of the highly seasonal nature of rain at this location as shown in **Figure 2**,
345 with almost all the rain falling in the summer half year. Furthermore, compared to the seasonal cycle of
346 rainfall, there is a very limited seasonal cycle for temperature at this location, with the average daily
347 temperature of 33.3°C in November and 30.5°C in July (www.bom.gov.au). Therefore, combined with the
348 case of Adelaide for which the seasonal cycle was not significant, it is likely that using seasonality as the
349 basis for evaluating the implications of atmospheric temperature is only robust in cases where the
350 precipitation itself occurs across all the seasons.

351 To what extent does atmospheric temperature provide a surrogate measure for these effects? We answer
352 this question by regressing the fraction of rain falling in the maximum six minute burst against both the day
353 of year and the maximum 2m near-surface temperature, to see whether the results in **Figure 4** can be
354 accounted for by temperature. The other measures of daily to sub-daily scaling were also evaluated and
355 found to be consistent; furthermore other metrics of surface temperature (e.g. average daily surface
356 temperature) were considered and once again led to similar results.

357 The results are shown in **Figure 5**, presented as a contour plot for each station, with the contours
358 representing the fraction of daily rainfall in the maximum six minute storm burst. In almost all cases the
359 results show much stronger gradients in the direction of temperature, and smaller gradients in the direction
360 of the day of year, highlighting that most of the seasonal variation in the daily to sub-daily scaling is
361 accounted for by the single metric of daily temperature. These results are consistent with the results of
362 Beuchat *et al*. [2011], who also found that seasonality could be accounted for by regressing against a range
363 of atmospheric covariates including temperature. In the case of Sydney, Brisbane and Hobart the seasonal
364 cycle after correcting for temperature differences has been almost entirely eliminated. In the case of Perth
365 and Melbourne, the corrected seasonal cycle becomes somewhat obscured and no longer clearly
366 interpretable, with the maxima in both locations conditional to a constant temperature occurring around

day 250 (September) and a local maxima for Perth around April, whereas for Melbourne the fraction of rainfall occurring as the maximum six minute burst is similar in both mid-winter and mid-summer. Similarly, Canberra shows its minima in late spring, which no longer reflects the seasonality shown in **Figure 4**. Once again since the day of year was not significant for Adelaide, the results for Adelaide were not shown here. The only two locations which still have a seasonal cycle are the tropical locations of Darwin and Cairns, which as discussed earlier are highly seasonal and do not have significant rain falling in the winter months. Interestingly for the case of Cairns, the impact of the seasonal cycle conditional to a constant atmospheric temperature now shows a higher fraction of rain falling in the maxima six minute burst during winter, which is the reverse of what was shown in **Figure 4**.

These results support the hypothesis which forms the basis for this paper: namely that information on atmospheric temperature (and, later, other atmospheric variables) can be used to infer the likely scaling properties between daily and sub-daily precipitation. In particular, despite the diversity of precipitation generating mechanisms which occur during the course of a year [*Evans and Westra*, 2012], much of the information important to disaggregating daily rainfall is contained within the single predictor of atmospheric temperature. This suggests that a similar logic might also be useful for inference about changes in the daily to sub-daily scaling relationship as the temperature warms under a future climate.

To further test this hypothesis, we examine the extent to which the different daily to sub-daily rainfall scaling relationships at each location can be accounted for by atmospheric temperature. This is done by setting up a GAM as a function of three predictors: the station (represented as a factor variable in the model), the maximum daily temperature, and the daily total rainfall amount. This latter predictor was included because of the significant difference in total daily rainfall between the different stations, and the fact that the proportion of rain falling in the maximum six minute storm burst itself varies with daily rainfall [*Westra et al.*, 2012]. The results are then presented: (a) conditional to the maximum daily temperature averaged at *each* station; and (b) conditional to the maximum daily temperature averaged *across all* the stations. The daily rainfall was held at its average value across all stations to eliminate the effect of variability in this predictor on the results.

393 The results are shown in **Figure 6** together with error bars representing ± two standard errors from the
394 point estimate. As can be seen, the upper panel, which represents the results conditional to maximum
395 temperature averaged at each station, shows a large range in the scaling relationship, with Darwin having
396 the largest fraction of rain falling in the maximum six minute burst and Hobart having the smallest, and with
397 the remaining stations showing intermediate values ranked approximately according to their latitude and
398 mean atmospheric temperature.

399 By contrast when looking at the results conditional to the maximum daily temperature averaged across all
400 locations (approximately 20°C; lower panel), the results show a much more consistent predicted response,
401 with most of the point estimates being within the confidence intervals of the other locations. Furthermore,
402 the change in the scaling relationship no longer shows any obvious relationship with latitude, with Hobart
403 still having the lowest scaling relationship but with Cairns showing the second lowest, whereas Perth has
404 the highest scaling relationship. The convergence in the daily to sub-daily rainfall scaling relationships by
405 conditioning on the same atmospheric temperature at each location is remarkable, given the distinct
406 climatology and seasonality of each region, and once again adds support to the hypothesis that much of the
407 information on daily to sub-daily scaling relationships can be accounted for by a small subset of
408 atmospheric predictors.

409 **4.2. Effect of incorporating additional atmospheric predictors in the model**

410 In the previous section it was shown that much of the variability between seasons and stations can be
411 accounted for by a single predictor representing atmospheric temperature. However, as suggested by other
412 studies [*Hardwick-Jones et al.*, 2010; *Utsumi et al.*, 2011], a range of atmospheric covariates such as the
413 availability of atmospheric moisture may also play an important role, and thus a more complete analysis is
414 now provided.

415 The flexibility of the GAM framework enables the formulation of a large number of plausible models, and a
416 diversity of predictor selection techniques exist for identifying statistically significant covariates. In this study
417 we use two predictor selection techniques to obtain two different predictor sets, and evaluate the
418 sensitivity of our results to the predictor selection approach. The first technique is backwards selection, in

419 which we begin with the full model and remove the least significant predictor (measured by the predictor's
420 *p* value). The model is then refitted with all the remaining predictors, and the process of removing
421 predictors is repeated until all predictors have a *p* value < 0.05. The second technique is available as part of
422 the *mgcv* R statistical package, and uses the restricted maximum likelihood approach (REML) described in
423 Wood [2006], which accounts for biases in the variance parameters as the number of model parameters
424 increases.

425 The results are summarised in **Table 3**. In addition to comparing the results of two predictor selection
426 approaches, we use three 'pools' of covariates for the model. The first pool includes only the daily rainfall
427 total, and the model was fitted using this covariate to provide a 'benchmark' level of model performance.
428 The reason for commencing with this covariate is that the daily to sub-daily rainfall scaling is known to co-
429 vary with the total daily rainfall amount [*Westra et al.*, 2012], and the inclusion of this predictor in all the
430 models will ensure that emphasis is placed on the model improvement after accounting for daily rainfall.
431 The second pool of predictors uses all the atmospheric temperature covariates to evaluate the influence of
432 atmospheric temperature on daily to sub-daily rainfall scaling. The final pool uses all the available
433 atmospheric predictors.

434 The model was fitted using tensor product smooths based on thin plate smoothing splines. It is noted that
435 all the models shown in **Table 3** only consider the additive effects of each of the predictors, such that their
436 interactions were not simulated. The reason for this was largely computational, since simulating the
437 interactions of more than five predictors resulted in significant computer memory limitations. To ensure
438 that this assumption did not significantly impact on our results, for several of the stations analysed we
439 continued with our backwards predictor selection by excluding all variables with a stricter threshold *p* value
440 of 0.001, resulting in five or less predictors. We then fitted the joint model using the multivariate tensor
441 product smooth, and found that this did not substantially improve the model performance, or result in
442 different conclusions to those presented later in this paper. Therefore focusing on the additive effects of
443 each predictor appears to be reasonable.

444 Finally we summarise our model performance using the adjusted R^2 (with the adjustment accounting for
445 the effective degrees of freedom of the model), and the proportion deviance explained is a generalisation of
446 the R^2 statistic. These statistics are also provided in **Table 3**, and a large improvement in model performance
447 can be observed by going from the daily rainfall-only model to the model which includes all the
448 temperature covariates, while moving from the temperature-only covariates to the full model yields a much
449 smaller improvement. Although the question of the 'optimal' predictor selection approach can be refined
450 further, in this paper we take the approach of retaining the multiple models, and evaluating the sensitivity
451 of model predictions to the individual model specification.

452 **4.3. GAM-MoF model evaluation**

453 In the previous sections we fitted the GAM model to a range of atmospheric covariates, and showed that
454 these covariates are able to account for a significant portion of the information on daily to sub-daily scaling
455 of rainfall. We now use the fitted GAM as the basis for applying the MoF algorithm given in Section 3.3 in
456 generating the full sub-daily temporal pattern conditional on historical atmospheric state. We evaluate the
457 performance of this model by generating the full sub-daily temporal pattern of rainfall for each day by using
458 the historical (reanalysis) data on atmospheric covariates for each wet day, and sampling the sub-daily
459 rainfall pattern from the next most similar day in terms of those covariates. For example we might be
460 interested in the sub-daily rainfall pattern on the 3rd of February 1979 at a particular location. We then use
461 the GAM to identify the similarity between that day and all the other days over the historical record, and we
462 might find that the next most similar day (in terms of the atmospheric temperature, relative humidity, sea
463 level pressure and so on) was the 23rd of December 2000. We then sample from this day, and repeat the
464 analysis for all remaining days of the record.

465 We conducted this analysis for each location, using the models obtained after conducting backward
466 selection as summarised in **Table 3**. The results are provided in **Table 4**, for a range of scales of aggregation
467 from six minutes through to 12 hours. The data is presented conditional to total daily rainfall, and therefore
468 results at longer time-scales will be identical to the historical record by construction. The results are
469 presented for the median of both the historical and simulated data, and are generally in good agreement.

Results for the 5% and 95%iles were also evaluated (not shown), and were found to be similar, indicating that the model is capable of reproducing the historical sub-daily rainfall patterns at each location conditional to the atmospheric covariates being sufficiently similar.

4.4. Evaluating the sensitivity to changes in atmospheric temperature

We now test the implications of changing the temperature-based covariates identified above to understand the sensitivity of the scaling relationship. We focus on the relationship between the daily rainfall and the fraction of rain falling in the maximum six minute storm burst, and evaluate the sensitivity to the covariates by increasing each of the atmospheric temperature variables by a specified amount while holding all other variables constant.

The results are summarised in **Table 5** for all three models, and **Figures 7** and **8** for the temperature-only model and the full model using the *mgcv* predictor selection algorithm, respectively. The results are provided both for the GAM-only model, in which the value of the covariate is obtained directly from the model, and from the GAM-MoF model, in which the GAM model is used to identify 'similar' days over the historical record, and one of those days selected for resampling. In the latter case the metrics (fraction of rainfall occurring in the maximum six minute and one hour storm bursts, and the fraction of the day with no rainfall) are then re-calculated from this full sub-daily temporal distribution.

Referring firstly to the temperature-only covariates using the GAM-only model, there was an increase in the fraction of rainfall occurring in the maximum six minute burst by between 2% (Melbourne) and 8% (Cairns) per degree change in atmospheric temperature, with a mean of 5% across all the stations. This implies a corresponding decrease in the rainfall occurring throughout the rest of the day, expressed either as a lower rainfall intensity during the remainder of the day or as a greater proportion of the day being dry. Comparing these results with those using the full GAM-MoF model for the six minute rainfall, the results are fairly comparable, although the GAM-MoF scaling is slightly less sensitive to temperature compared with the GAM-only scaling. For example, the mean sensitivity was found to be 4.1% using only the temperature covariates compared with 5% using the GAM directly. Similar results can be observed by comparing **Figure 7b** with **Figure 7a**, with the absolute magnitude of the scaling being slightly lower, but the stations which

496 show higher (lower) scaling for the GAM also show higher (lower) scaling for the GAM-MoF approach.

497 These results can be contrasted to the results using the complete pool of predictors listed in **Table 2**. We
498 again test the sensitivity of changes to atmospheric temperature, but this time hold the remaining variables
499 at their mean values. This yields a substantial increase in the percentage change in rainfall occurring in the
500 maximum six minute burst across all stations, with the backwards selection algorithm for the GAM-only
501 model showing a mean/median increase of 13.4%/9.0% per degree, respectively, while the *mgcv* predictor
502 selection algorithm gives increases of 9.5%/11.0%. This is approximately double the case for the
503 temperature only predictor, and highlights that even though the improvement of model performance as
504 indicated by the adjusted R^2 statistic or deviance statistic in **Table 3** is relatively small, the impacts on model
505 predictions can be significant. In addition to an increase in the average across all stations, the range of
506 results between stations also increased dramatically, ranging from -6% in Canberra to +38% in Adelaide.

507 Considering the remaining metrics using the GAM-MoF algorithm, the fraction of rain falling in the
508 maximum one hour burst has a scaling which is about two thirds the scaling for the maximum six minute
509 burst, while fraction of day with no rainfall only increases by about 1.5% per degree change in temperature
510 for the temperature-only covariates, and 3.1% / 2.4% for the backwards selection and *mgcv* predictor
511 selection approaches, respectively. This suggests that although the full distribution of sub-daily rainfall is
512 expected to change as a result of anthropogenic climate change, the greatest sensitivity is for the intensity
513 of rainfall over very short timescales.

514 The decrease of 3% and 6% per degree for the backwards selection and *mgcv* approach, respectively, in
515 Canberra represents the only case where the sensitivity to temperature was negative. This was not
516 observed for the temperature-only model, for which the fraction of daily rainfall occurring in the maximum
517 six minute burst increased by 5%, suggesting that interactions with non-temperature covariates are causing
518 the change in sign. We repeated the predictor selection using the *mgcv* default predictor selection
519 algorithm, but removing individual covariates from the pool of predictors to determine what is causing the
520 observed decline. It was found that removing the relative humidity covariates but retaining all other non-

521 temperature atmospheric covariates yielded results which were once again consistent with the results using
522 temperature-only covariates: namely an increase of 5% per degree. Interestingly, the R^2 and deviance
523 statistics were 0.279 and 37.7%, respectively, compared with 0.281 and 38.2% for the full model, suggesting
524 that removing relative humidity had only marginal impact on overall model performance, with this being
525 partly attributable to the significant co-variation between temperature and relative humidity at all the
526 locations analysed. The fact that the selection of different predictors can lead to very different projections is
527 an issue which does not just affect this disaggregation algorithm but affects statistical downscaling
528 algorithms more generally [*Fowler et al.*, 2007; *Timbal et al.*, 2008], and we return to this issue in the
529 discussion and conclusions section.

530 Lastly, we examine changes to the average annual maximum rainfall intensity for both the six minute and
531 one hour storm bursts. Annual maximum rainfall is often used as the basis for flood frequency estimation,
532 and therefore we are interested in how this might change in the future. To derive the annual maximum
533 intensities, the re-sampled fraction of rainfall occurring in the maximum six minute and one hour bursts is
534 simply multiplied by the original sequence of daily rainfall amounts, to recover the rainfall as a depth falling
535 over that time increment. For each year of record, the maximum intensity is selected, and this is repeated
536 for the 28 years of record (from 1979 to 2006). This is repeated for changes to atmospheric temperature
537 from -3°C to +3°C, and the average sensitivity per degree change in temperature is then calculated. It is
538 important to note that these results are presented conditional to daily rainfall intensity staying the same; as
539 discussed in the introduction, to develop complete projections of annual maximum rainfall will require
540 coupling to a daily rainfall downscaling algorithm.

541 These results are shown in **Table 6**. Only the results using the *mgcv* / REML predictor selection algorithm are
542 presented, and the results for changes to annual maximum rainfall show very strong consistency with the
543 results from **Table 5**, suggesting that – at least according to the results of this statistical disaggregation
544 algorithm – the climate sensitivity is more clearly related to the timescale of the precipitation event, rather
545 than to how extreme it is. However it should be cautioned that this may partly be due to the fact that the
546 GAM was fit to all the data rather than just the extremes, such that it is more likely to reflect changes in

547 average daily to sub-daily behaviour rather than just the highest percentiles.

548 To conclude, we emphasise that the overarching result of this sensitivity analysis is that, with the possible
549 exception of Canberra, all the models consistently show increases in the six minute rainfall intensity with
550 temperature, even if the magnitude of increase differed between models and locations. This conforms with
551 our general expectations of changes in precipitation characteristics under a future climate, which Trenberth
552 [2011] refers to as the *'it never rains but it pours*' syndrome of a future climate having more intense rainfall
553 interspersed by longer dry periods. The interesting result of this research is the extent to which this
554 translates to the sub-daily timescale, with potential increases of around 5-10% or more in the intensity of
555 very short storm bursts per degree change in atmospheric temperature, independent of any change to daily
556 rainfall. If changes to daily rainfall characteristics also conform to this general pattern of fewer wet days and
557 increased intensity per wet day, then this will compound the effect, highlighting the significant sensitivity of
558 the shortest-duration rainfall events to changes in atmospheric temperature.

559 ## 5. Discussion and conclusions

560 This paper provides a framework for disaggregating daily rainfall into sub-daily rainfall fragments, which can
561 be estimated for any temporal resolution of interest provided that historical records are available at that
562 resolution. In Australia, the sub-daily data was digitised at a resolution of 0.1 hour (6 minutes), and thus this
563 was the finest resolution considered here. Conceptually the algorithm presented in this paper can be made
564 to work at any location for which adequate sub-daily rainfall is available, and this potentially can be
565 generalised to any location regardless of the availability of sub-daily information using the algorithm
566 described in Westra et al. [2012] and Mehrotra et al. [2012].

567 The basis of the algorithm is that the scaling relationships between daily and sub-daily rainfall can be
568 accounted for by knowing the daily rainfall amount, and the historical and future values of a set of
569 atmospheric predictors. As discussed in the introduction, it is difficult to 'validate' any downscaling model
570 given the limited temperature changes over the historical record compared with what is projected in the
571 future. As an alternative, we hypothesise that if the daily to sub-daily scaling relationship – which is known

572 to vary seasonally and from one location to another - can be accounted for largely by the atmospheric
573 covariates, then this suggests that future changes in daily to sub-daily scaling as a result of climate change
574 can also be described by changes in these covariates. This hypothesis was found to be reasonable using
575 three metrics of daily to sub-daily scaling, with almost all the seasonality eliminated at many of the
576 locations, and the scaling relationships at very different locations such as Darwin and Hobart were found to
577 converge substantially after accounting for atmospheric temperature.

578 We examined different generalised additive model structures, and found that reasonable model
579 performance occurred simply as a function of daily rainfall amount and a set of atmospheric temperature-
580 based covariates. We also fitted other atmospheric covariates including dew point temperature, relative
581 humidity, wind strength and direction, mean sea level pressure and geopotential height, and found a small
582 but significant additional improvement (*i.e.* a small increase in the adjusted R^2 or the deviance explained) in
583 model performance.

584 The sensitivity to a change in atmospheric temperature was evaluated by adjusting all the atmospheric
585 temperature covariates by between -3°C and +3°C, and then calculating the average change in daily to sub-
586 daily scaling metrics per degree temperature change. The sensitivity was found to be highest for the
587 shortest duration rainfall, of about 5% per degree using the temperature-only covariates, and about double
588 this using all covariates. This latter result is due to the strong negative correlation between atmospheric
589 temperature and relative humidity, so that future projections of atmospheric moisture will have an
590 important impact on projections of changes to rainfall intensity. The conclusion that the intensity of the
591 shortest-durations rainfall events will increase as temperature increases appears to be robust for a wide
592 range of choices of covariates, although the absolute magnitude of the change varied depending on the
593 model specification. The only exception was for Canberra due to interactions with the relative humidity
594 covariate, although further research, perhaps using dynamical model outputs, is required to better
595 understand this anomaly.

596 Finally, we demonstrated the extension to the MoF logic to disaggregate daily rainfall under a future climate.

597 The algorithm uses the fitted GAM as the basis for selecting days with 'similar' atmospheric covariates
598 compared to what is expected in the future, and this was trailed through a sensitivity assessment by
599 changing atmospheric temperature while holding all the other atmospheric covariates constant. The results
600 were found to be consistent with using the GAM directly, with the benefit of using the disaggregation logic
601 being that the full distribution of rainfall over the course of the day can be simulated. In this case only the
602 fraction of rain falling in the maximum six minute and one hour bursts, and the fraction of the day with no
603 rainfall, were evaluated. However, a diversity of other sub-daily rainfall statistics can easily be assessed as
604 well, including information of other storm burst durations, the temporal pattern, and information on the
605 diurnal cycle of rainfall.

606 In the future, we intend to couple the disaggregation algorithm described here with a daily downscaling
607 algorithm, to develop projections for sub-daily rainfall under a future climate. Given the sensitivity to
608 different predictor sets in the present analysis, such an algorithm must be developed to account both for
609 GCM uncertainty as well as uncertainty in the GAM predictor selection algorithm. In terms of the
610 disaggregation algorithm, such uncertainty could be estimated by generating an ensemble of projections
611 based on different plausible predictor sets that were found to perform well in precipitation hind-casts.

612 Despite this uncertainty, it is clear from the results presented in this paper that the temporal distribution of
613 sub-daily rainfall is highly sensitive to changes in atmospheric temperature and other atmospheric
614 covariates such as relative humidity, resulting in averaged increases across all stations of between 4.1% and
615 13.4% per degree change in temperature for the maximum six minute burst, between 3.1% and 6.8% for the
616 maximum one hour burst, and between 1.5% and 3.5% for the fraction of the day with no rainfall.
617 Furthermore, results from some of the individual stations showed changes to the scaling relationships much
618 greater than this. Assuming a temperature change of between 1.1°C and 6.4°C by the end of the 21st
619 Century as indicated by [*IPCC*, 2007], this indicates that we can expect potentially major changes to the
620 intensities and temporal patterns of sub-daily rainfall, with potentially significant implications on a vast
621 number of hydrological systems.

622

623 ## References

624 Alexander, L. V., et al. (2006), Global observed changes in daily climatic extremes of temperature and
625 precipitation, *Journal of Geophysical Research*, *111*(D05101).

626 Allan, R. P., and B. J. Soden (2008), Atmospheric warming and the amplification of precipitation extremes,
627 *Science*, *321*, 1481-1484.

628 Allan, R. P., B. J. Soden, V. O. John, W. Ingram, and P. Good (2010), Current changes in tropical precipitation,
629 *Environmental Research Letters*, *5*(025205).

630 Bates, B. C., Z. W. Kundzewicz, S. Wu, and J. P. Palutikof (2008), Climate Change and Water. Technical Paper
631 of the Intergovernmental Panel on Climate Change*Rep.*, 210 pp, IPCC Secretariat, Geneva.

632 Berg, P., J. O. Haerter, P. Thejll, C. Piani, S. Hagemann, and J. H. Christensen (2009), Seasonal characteristics
633 of the relationship between daily precipitation intensity and surface temperature, *Journal of Geophysical*
634 *Research*, *114*(D18102).

635 Beuchat, X., B. Schaefli, M. Soutter, and A. Mermoud (2011), Toward a robust method for subdaily rainfall
636 downscaling from daily data, *Water Resources Research*, *47*(W09524).

637 Charles, S. P., B. C. Bates, and J. P. Hughes (1999a), A spatio-temporal model for downscaling precipitation
638 occurrence and amounts, *Journal of Geophysical Research*, *104*(D24), 31657-31669.

639 Charles, S. P., B. C. Bates, P. H. Whetton, and J. P. Hughes (1999b), Validation of downscaling models for
640 changed climate conditions: case study of southwestern Australia, *Climate Research*, *12*, 1-14.

641 Evans, J., and S. Westra (2012), Investigating the Mechanisms of Diurnal Rainfall Variability using a Regional
642 Climate Model, *Journal of Climate*, *25*(20), 7232-7247.

643 Fowler, H. J., S. Blenkinsop, and C. Tebaldi (2007), Linking climate change modelling to impact studies:
644 Recent advances in downscaling techniques for hydrological modelling, *International Journal of Climatology*,
645 *27*, 1547-1578.

646 Gleason, B., P. Y. Groisman, T. C. Peterson, R. Vose, and R. Ezell (2002), A new global daily temperature and
647 precipitation dataset, in *13th Symposium on Global Change and Climate Variations, American*
648 *Meteorological Society*, edited, Orlando.

649 Haerter, J. O., and P. Berg (2009), Unexpected rise in extreme precipitation caused by a shift in rain type?,
650 *Nature Geoscience*, *2*, 372-373.

651 Haerter, J. O., P. Berg, and S. Hagemann (2010), Heavy rain intensity distributions on varying time scales and
652 at different temperatures, *Journal of Geophysical Research*, *115*(D17102).

653 Hardwick-Jones, R., S. Westra, and A. Sharma (2010), Observed relationships between extreme sub-daily

precipitation, surface temperature and relative humidity, *Geophysical Research Letters*, *37*(L22805).

Hastie, T., and R. Tibshirani (1986), Generalized additive models (with discussion), *Statistical Science*, *1*, 297-318.

Hastie, T., and R. Tibshirani (1990), *Generalized Additive Models*, London.

IPCC (2007), Climate Change 2007: Synthesis Report. Contribution of Working Groups I, II and III to the Fourth Assessment Report of the Intergovernmental Panel on Climate Change*Rep.*, 104 pp, IPCC, Geneva, Switzerland.

IPCC (2011), Summary for Policymakers. In: Intergovernmental Panel on Climate Change Special Report on Managing the Risks of Extreme Events and Disasters to Advance Climate Change Adaptation*Rep.*, Cambridge University Press, Cambridge, United Kingdom, and New York, NY, USA.

Jakob, D., D. J. Karoly, and A. Seed (2011), Non-stationarity in daily and sub-daily intense rainfall - Part 2: Regional assessment for sites in south-east Australia, *National Hazards and Earth Systems Science*, *11*, 2273-2284.

Johnson, F., and A. Sharma (2009), Measurement of GCM skill in predicting variables for hydroclimatological assessments, *Journal of Climate*.

Klein Tank, A. M. G., J. B. Wijngaard, and 37 co-authors (2002), Daily dataset of 20th century surface air temperature and precipitation series for the European Climate Assessment, *International Journal of Climatology*, *22*, 1441-1453.

Lenderink, G., and E. van Meijgaard (2008), Increase in hourly precipitation extremes beyond expectations from temperature changes, *Nature Geoscience*, *1*, 511-514.

Lenderink, G., H. Y. Mok, T. C. Lee, and G. J. Van Oldenborgh (2011), Scaling and trends of hourly precipitation extremes in two different climate zones - Hong Kong and the Netherlands, *Hydrological Earth Systems Science*, *8*, 4701-4719.

Mehrotra, R., and A. Sharma (2006), A nonparametric stochastic downscaling framework for daily rainfall at multiple locations, *Journal of Geophysical Research*, *111*(D15101).

Mehrotra, R., and A. Sharma (2007), Preserving low-frequency variability in generated daily rainfall sequences, *Journal of Hydrology*, *345*, 102-120.

Mehrotra, R., and A. Sharma (2010), Development and application of a multisite rainfall stochastic downscaling framework for climate change impact assessment, *Water Resources Research*, *46*(W07526).

Mehrotra, R., S. Westra, A. Sharma, and R. Srikanthan (2012), Continuous Rainfall Simulation: 2 - A regionalised daily rainfall generation approach, *Water Resources Research 48*(W01536).

Muller, C. J., P. A. O'Gorman, and L. E. Back (2011), Intensification of Precipitation Extremes with Warming in a Cloud Resolving Model, *Journal of Climate*, *24*, 2784-2800.

687 Peterson, T. C., H. Daan, and P. D. Jones (1997), Initial selection of a GCOS surface network, *Bulletin of the*
688 *American Meteorological Society*, *78*, 2837-2849.

689 Romps, D. M. (2011), Response of Tropical Precipitation to Global Warming, *Journal of the Atmospheric*
690 *Sciences*, *68*, 123-138.

691 Saha, S., S. Moorthi, H.-L. Pan, and e. al (2010), The NCEP Climate Forecast System Reanalysis, *Bulletin of the*
692 *American Meteorological Society*, 43.

693 Semenov, M. A., and E. M. Barrow (1997), Use of a stochastic weather generator in the development of
694 climate change scenarios, *Climatic Change*, *35*, 397-414.

695 Semenov, M. A., and P. Stratonovitch (2010), Use of multi-model ensembles from global climate models for
696 assessment of climate change impacts, *Climate Research*, *41*, 1-14.

697 Timbal, B., P. Hope, and S. Charles (2008), Evaluating the consistency between statistically downscaled and
698 global dynamical model climate change projections, *Journal of Climate*, *21*(22), 6052-6059.

699 Trenberth, K. E. (2011), Changes in precipitation with climate change, *Climate Research*, *47*, 123-138.

700 Trenberth, K. E., A. Dai, R. M. Rasmussen, and D. B. Parsons (2003), The changing character of precipitation,
701 *Bulletin of the American Meteorological Society*, *84*, 1205-1217.

702 Utsumi, N., S. Seto, S. Kanae, E. E. Maeda, and T. Oki (2011), Does higher surface temperature intensify
703 extreme precipitation?, *Geophysical Research Letters*, *38*(L16708).

704 Wallace, J. M., and P. V. Hobbs (2006), *Atmospheric Science: An Introductory Survey*, 2nd edition ed.

705 Westra, S., and S. A. Sisson (2011), Detection of non-stationarity in precipitation extremes using a max-
706 stable process model, *Journal of Hydrology*, *406*, 119-128.

707 Westra, S., R. Mehrotra, A. Sharma, and R. Srikanthan (2012), Continuous Rainfall Simulation: 1 - A
708 regionalised sub-daily disaggregation approach, *Water Resources Research*, *48*(W01535).

709 Wood, S. N. (2006), *Generalized Additive Models: An Introduction with R*, 392 pp.

710

711

712

713 List of Figure Captions

714 Figure 1: Map of Australia with location of gauges used for the analysis.

715 Figure 2: Series of monthly rainfall totals (solid lines, left axis) and the average monthly rainfall intensity
716 (mm/day) during wet days (dashed lines, right axis).

717 Figure 3: Schematic diagram of the GAM-MoF algorithm, with the sub-daily temporal patterns going from
718 constant rainfall occurring over the full day (pattern 1) through to high intensity rainfall occurring over only
719 a small portion of the day (pattern 3). It is hypothesised that a warmer atmosphere will lead to a
720 progression from pattern 1 to pattern 3, and the GAM-MoF algorithm will therefore increasingly sample
721 from such days as the atmosphere warms. Steps 1 to 4 relate to the steps described in Section 3.1.

722 Figure 4: Variability of fraction of daily rain falling in maximum 6-minute (left panel) and 1-hour (middle
723 panel), and fraction of day with no rainfall (right panel), against the day of the year. Only stations which had
724 a statistically significant seasonal cycle were presented.

725 Figure 5: Contour plot of fraction of rain falling as maximum 6 minute storm burst, against maximum 2m
726 daily temperature (x axis) and day of year (y axis).

727 Figure 6: Fraction of rain falling in maximum 6 minute storm burst as a function of station, with the
728 atmospheric temperature set at the mean at each station (upper panel) and the mean across all stations
729 (lower panel). In all cases the daily rainfall amount was set at the mean across all stations. The intervals
730 represent ± 2 standard deviations from the fitted model value.

731 Figure 7: Change in different metrics of daily to sub-daily scaling as a function of changes in atmospheric
732 temperature, simulating directly from the fitted GAM (left panel) or extracted after running the method of
733 fragments approach but conditionally sampling on different atmospheric temperatures. Results using
734 temperature-only covariates.

735 Figure 8: Change in different metrics of daily to sub-daily scaling as a function of changes in atmospheric
736 temperature, simulating directly from the fitted GAM (left panel) or extracted after running the method of
737 fragments approach but conditionally sampling on different atmospheric temperatures. Results using
738 covariates fitted via the *mgcv* predictor selection algorithm.

739
740

741

742 ## Tables

Table 1: *Rainfall dataset used for the analysis.*

Location	Gauge name and number	Latitude	Longitude
Perth	009021 (Perth Airport)	-31.93	115.98
Darwin	014015 (Darwin Airport)	-12.42	130.89
Adelaide	023034 (Adelaide Airport)	-34.95	138.52
Cairns	031011 (Cairns Airport)	-16.87	145.74
Brisbane	040223 (Brisbane Airport)	-27.42	153.11
Sydney	066062 (Sydney Observatory Hill)	-33.86	151.21
Canberra	070014 (Canberra Airport)	-35.30	149.20
Melbourne	086071 (Melbourne Regional Office)	-37.81	144.97
Hobart	094029 (Hobart, Ellerslie Rd)	-42.89	147.33

743

744

745

Table 2: *Summary of variables extracted from the CFSR reanalysis at the grid point closest to the station locations in Table 1.*

Variable	**Abbreviated name**	**Daily mean, maxima, minima and/or diurnal range**	**Units**
Daily total precipitation	P_daily	mean	mm
2m surface temperature	t2m, t2m_max, t2m_min, t2m_range	mean, maxima, minima, range	Degrees Celsius
500, 700 and 850hPa temperature	t500, t700, t850	mean	Degrees Celsius
Dew point temperature	Td_max	maxima	Degrees Celsius
Relative humidity	RH, RH_max	mean and maxima	Percentage (%)
Pressure reduced to mean sea level	Prmsl, Prmsl_min	mean and minima	Pa
850hPa wind strength and direction	wnd850_str, wnd850_dir	mean	(derived from *u* and *v* components of wind; units of m/s)
10m wind strength and direction	wnd10m_str, wnd10m_dir	mean	(derived from *u* and *v* components of wind; units of m/s)
500 and 850hPa geopotential height	z500, z850	mean	Geopotential meter (gpm)

746

747

748

Table 3: *Predictor selection using a generalised additive model with tensor product splines as the smoothing function. Predictor selection was conducted separately for each station, using the fraction of daily total rain falling in the maximum 6 minute burst as the response variable. Backward selection was used for variable selection, with three pools of variables: daily rainfall only (serving as the 'benchmark' for comparison purposes), daily rainfall and atmospheric temperature variables only, and all variables. The following covariate pools were used:* ***A*** *(daily rainfall only),* ***B*** *(temperature variables and daily rainfall only, using backwards selection),* ***C*** *(all variables, using backwards predictor selection) and* ***D*** *(all variables, using mgcv algorithm with REML for predictor selection).*

Station	**Covariate pool**	**Covariates identified through backward selection**	**Model performance metrics. First number is the adjusted R^2, and second number is the deviance explained.**
Perth	A	P_daily	0.272, 31.4%
	B	P_daily, tmp2m, tmp2m_min, t500	0.314, 37.5%
	C	P_daily, tmp2m, tmp2m_min, tmp2m_range, t500, t700, RH, wnd10m_str, z500, z850	0.324, 39.7%
	D	P_daily, tmp2m_max, tmp2m_min, t500, t700, t850, RH, RH_max, prmsl_min, z500, z850	0.327, 38.7%
Darwin	A	P_daily	0.277, 33.3%
	B	P_daily, tmp2m, tmp2m_max, t700, t850	0.365, 42.8%
	C	P_daily, t500, t700, t850, RH_max, wnd10m_str, z850	0.385, 44.1%
	D	P_daily, tmp2m, tmp2m_min, t500, t700, t850, RH_max, wnd850_str, wnd10m_str, z850	0.385, 44.3%
Adelaide	A	P_daily	0.207, 24.3%
	B	P_daily, tmp2m_min, t500	0.208, 26.4%
	C	P_daily, tmp2m_min, t500, t700, t850, max_Td, RH_max, wnd850_str, wnd10m_dir, z500, z850	0.258, 34.5%
	D	P_daily, tmp2m_max, t500, t700, t850, max_Td, RH, RH_max, prmsl, prmsl_min, wnd850_str, wnd850_dir, wnd10m_str, wnd10m_dir, z500, z850	0.260, 35.2%
Cairns	A	P_daily	0.295, 38.1%
	B	P_daily, tmp2m, tmp2m_max, tmp2m_min, t700	0.365, 48.6%
	C	P_daily, t500, max_Td, RH, prmsl, wnd850_str, wnd10m_str, z500, z850	0.375, 50.0%
	D	P_daily, t500, t850, max_Td, RH, prmsl,	0.380, 50.0%

		prmsl_min, wnd850_str, wnd10m_str, z500, z850	
Brisbane	A	P_daily	0.265, 29.4%
	B	P_daily, tmp2m, tmp2m_min, t500, t850	0.308, 43.3%
	C	P_daily, tmp2m_range, t700, t850, max_Td, RH, RH_max, prmsl, z500, z850	0.342, 47%
	D	P_daily, tmp2m, tmp2m_range, t500, t700, t850, Td, RH, RH_max, prmsl, prmsl_min, wnd10m_str, z500, z850	0.342, 47.3%
Sydney	A	P_daily	0.228, 27.0%
	B	P_daily, tmp2m, tmp2m_range, t500	0.244, 33.0%
	C	P_daily, t500, t700, t850, max_Td, RH, RH_max, prmsl, wnd850_str, wnd10m_str, z500, z850	0.304, 38.0%
	D	P_daily, tmp2m_max, max_Td, RH, RH_max, prmsl, prmsl_min, wnd850_str, wnd850_dir, wnd10m_str, z500, z850	0.294, 37.6%
Canberra	A	P_daily	0.173, 19.7%
	B	P_daily, tmp2m, tmp2m_max, t500, t700, t850	0.250, 35.6%
	C	P_daily, tmp2m_max, t500, RH, RH_max, prmsl_min, wnd850_dir, z500	0.281, 38.9%
	D	P_daily, tmp2m_range, t500, RH, RH_max, prmsl_min, wnd850_str, wnd10m_str, z500	0.281, 38.2% (note: without relative humidity predictors in pool, scores becomes 0.279, 37.7% - see discussion in **Section 3.4**)
Melbourne	A	P_daily	0.193, 22.0%
	B	P_daily, tmp2m_max, tmp2m_range, t700	0.223, 27.6%
	C	P_daily, tmp2m_max, t500, t700, RH_max, prmsl, z500, z850	0.250, 33.7%
	D	P_daily, tmp2m_max, t700, t850, RH, RH_max, prmsl_min, wnd850_str, wnd10m_dir, z500, z850	0.252, 33.3%
Hobart	A	P_daily	0.241, 33.0%
	B	P_daily, tmp2m, tmp2m_range, t500	0.284, 43.3%
	C	P_daily, tmp2m, tmp2m_range, t500, max_Td, RH, RH_max, wnd850_dir, wnd10m_str, wnd10m_dir	0.347, 48.3%
	D	P_daily, tmp2m, tmp2m_max, tmp2m_min, t500, max_Td, RH, RH_max, prmsl_min, wnd850_str, wnd850_dir, wnd10m_str, wnd10m_dir, z500	0.356, 49.1%

Table 4: *Validation statistics for the fraction of rain falling in the maximum 6 minute, 1 hour, 3 hour and 12 hour storm bursts, as well as the fraction of the daily with no rainfall. The left figure represents the median of the observed data, and the right figure (in parentheses) represents the median of the simulated data.*

	Max 6 min	**Max 1 hour**	**Max 3 hour**	**Max 12 hour**	**Frct zero rainfall**
Perth	0.165 (0.165)	0.424 (0.421)	0.636 (0.629)	0.986 (0.979)	0.733 (0.729)
Darwin	0.247 (0.246)	0.707 (0.679)	0.896 (0.882)	1.00 (1.00)	0.854 (0.850)
Adelaide	0.173 (0.175)	0.490 (0.478)	0.707 (0.695)	1.00 (0.999)	0.829 (0.825)
Cairns	0.165 (0.168)	0.485 (0.484)	0.666 (0.664)	0.996 (0.993)	0.771 (0.771)
Brisbane	0.174 (0.172)	0.530 (0.521)	0.732 (0.715)	1.00 (1.00)	0.829 (0.821)
Sydney	0.142 (0.137)	0.469 (0.459)	0.690 (0.687)	1.00 (1.00)	0.767 (0.762)
Canberra	0.125 (0.116)	0.469 (0.469)	0.725 (0.718)	1.00 (1.00)	0.783 (0.783)
Melbourne	0.142 (0.141)	0.485 (0.480)	0.725 (0.715)	1.00 (1.00)	0.812 (0.812)
Hobart	0.115 (0.113)	0.427 (0.428)	0.683 (0.676)	1.00 (1.00)	0.796 (0.790)

Table 5: *Percentage change in three attributes of daily to sub-daily rainfall scaling: fraction of rain falling in the maximum 6 minute and 1 hour bursts, and fraction of day with no rainfall, all represented per degree of atmospheric warming. The change in attributes were evaluated both using the output directly from the GAM, and using a modified Method of Fragments approach to generate more complete daily to sub-daily rainfall statistics. The models used based on the covariate pools described in* ***Table 3*** *were used to evaluate sensitivity of model selection.*

Station	Model	Fraction rainfall in maximum 6 minute burst - GAM	Fraction rainfall in maximum 6 minute burst - MoF	Fraction rainfall in maximum 1 hour burst - MoF	Fraction of day with no rainfall – MoF
Perth	B	4	5	4	2
	C	18	16	10	6
	D	11	12	9	5
Darwin	B	6	5	4	3
	C	9	9	7	4
	D	8	8	6	4
Adelaide	B	3	3	2	0
	C	38	29	16	6
	D	25	18	10	3
Cairns	B	8	6	5	3
	C	7	5	4	2
	D	11	8	7	3
Brisbane	B	7	4	3	1
	C	9	6	3	1
	D	12	7	5	2
Sydney	B	5	5	4	2
	C	9	11	6	3
	D	2	3	2	1
Canberra	B	5	4	2	1
	C	-3	-4	-2	-1
	D	-6	-4	-3	-1

Melbourne	B	2	1	1	0
	C	20	14	10	4
	D	13	10	7	2
Mean / median across all stations	B	5.0 / 5.0	4.1 / 4.5	3.1 / 3.5	1.5 / 1.5
	C	13.4 / 9.0	10.8 / 10.0	6.8 / 6.5	3.1 / 3.5
	D	9.5/ 11.0	7.8 / 8.0	5.4 / 6.5	2.4 / 2.5

Table 6: *Change in annual maximum 6 minute and 1 hour storm burst per degree change in the atmospheric temperature covariates, represented as a percentage. Results are shown for the* mgcv *algorithm predictor selection with REML only.*

Station	**Annual maximum 6 minute storm burst**	**Annual maximum 1 hour storm burst**
Perth	11.6	14.1
Darwin	6.0	4.7
Adelaide	22.3	9.5
Cairns	12.6	8.0
Brisbane	6.1	5.1
Sydney	6.0	3.3
Canberra	-6.7	-4.0
Melbourne	14.2	11.3
Hobart	7.6	1.9
Mean/ median across all stations	8.8 / 7.6	5.4 / 5.5

Figures

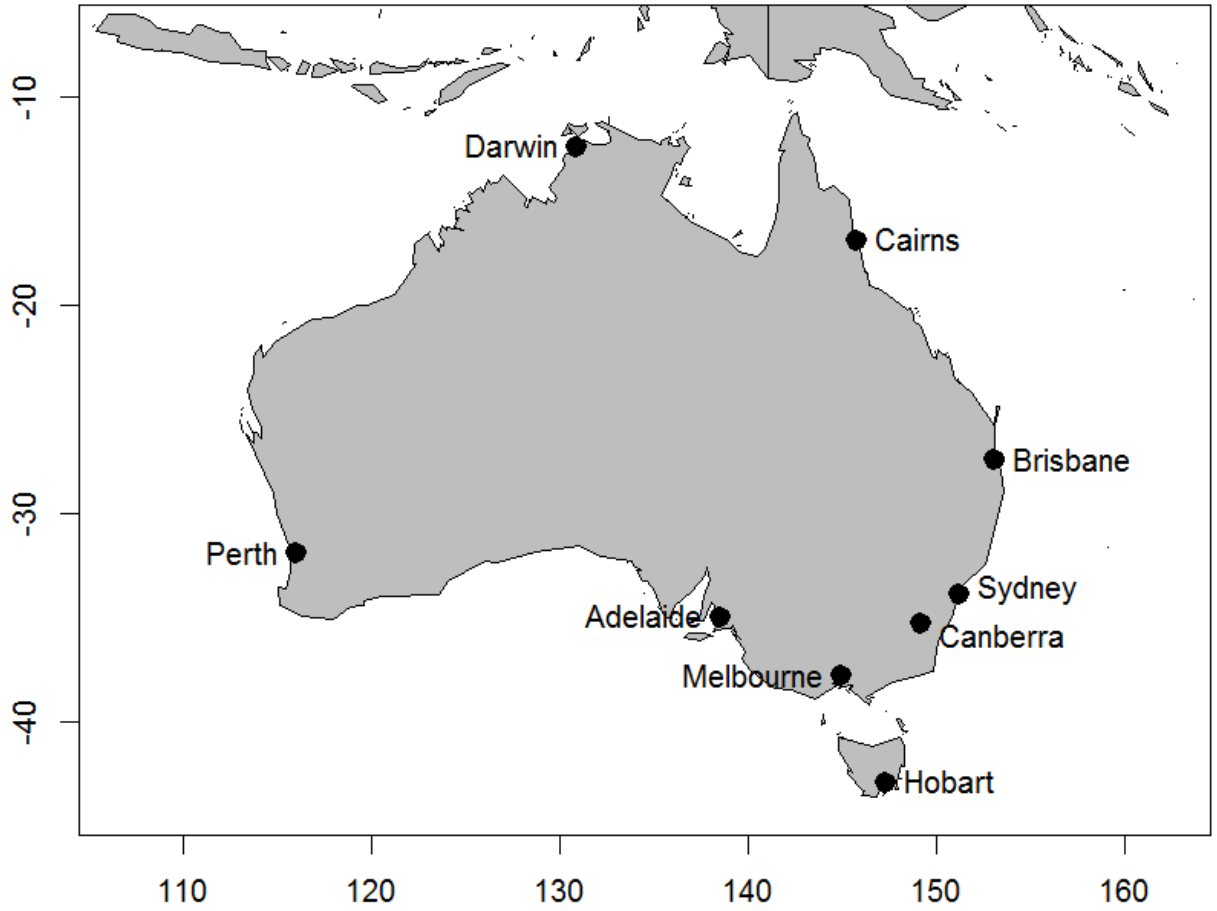

Figure 1: Map of Australia with location of gauges used for the analysis.

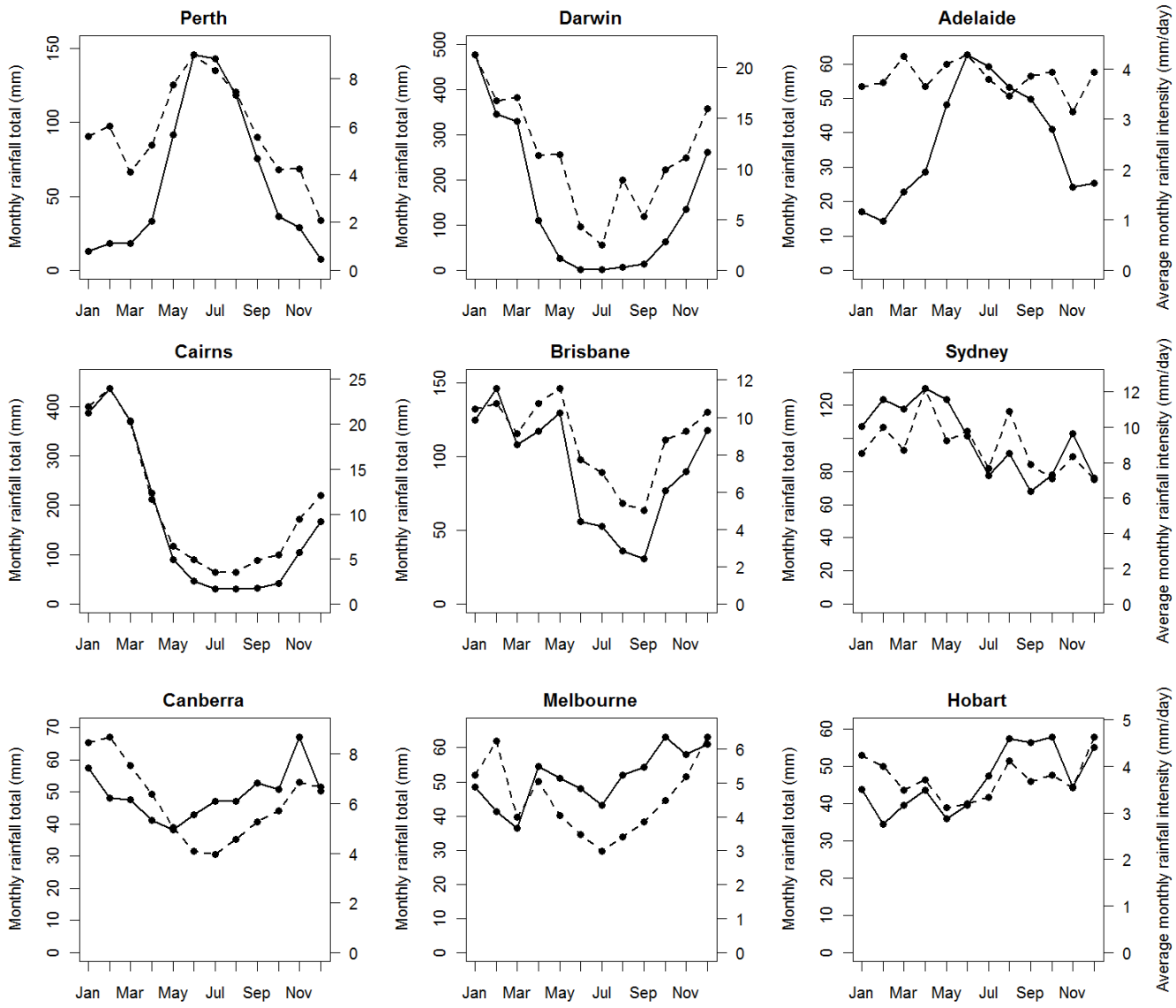

Figure 2: Series of monthly rainfall totals (solid lines, left axis) and the average monthly rainfall intensity (mm/day) during wet days (dashed lines, right axis).

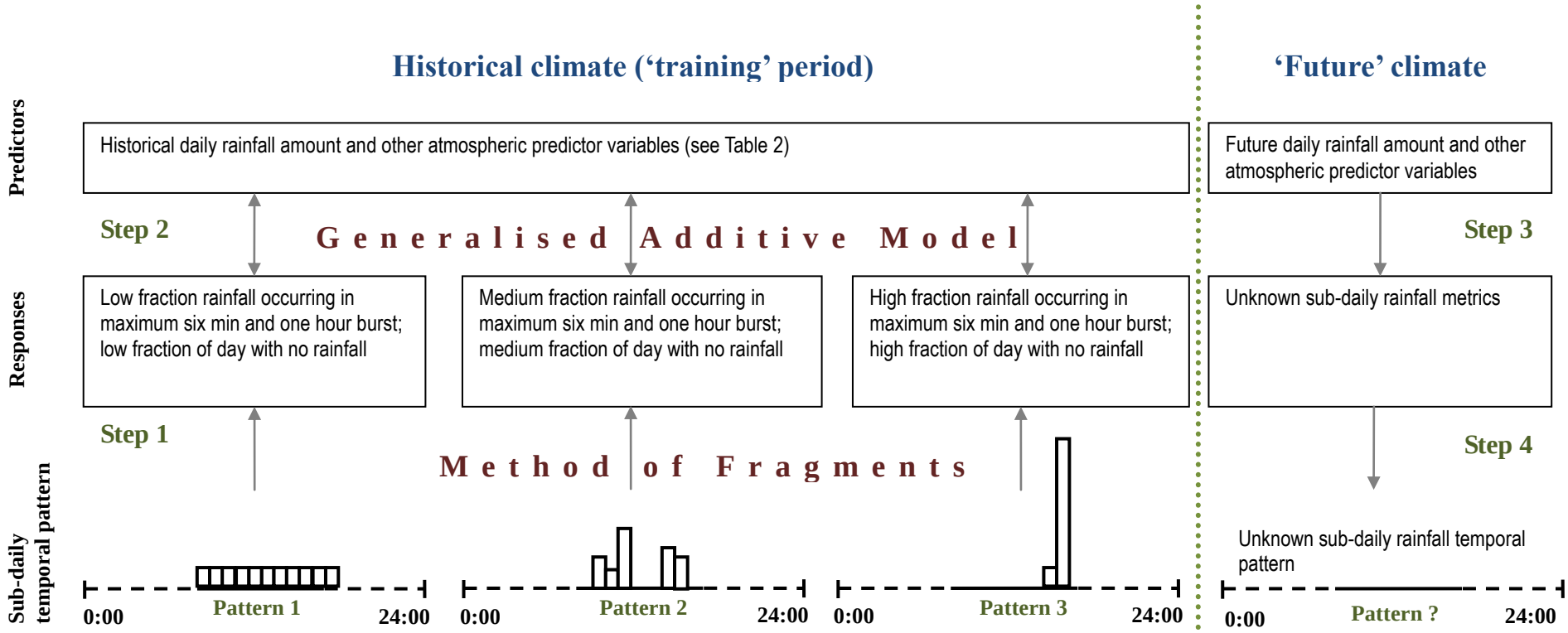

Figure 3: Schematic diagram of the GAM-MoF algorithm, with the sub-daily temporal patterns going from constant rainfall occurring over the full day (pattern 1) through to high intensity rainfall occurring over only a small portion of the day (pattern 3). It is hypothesised that a warmer atmosphere will lead to a progression from pattern 1 to pattern 3, and the GAM-MoF algorithm will therefore increasingly sample from such days as the atmosphere warms. Steps 1 to 4 relate to the steps described in Section 3.1.

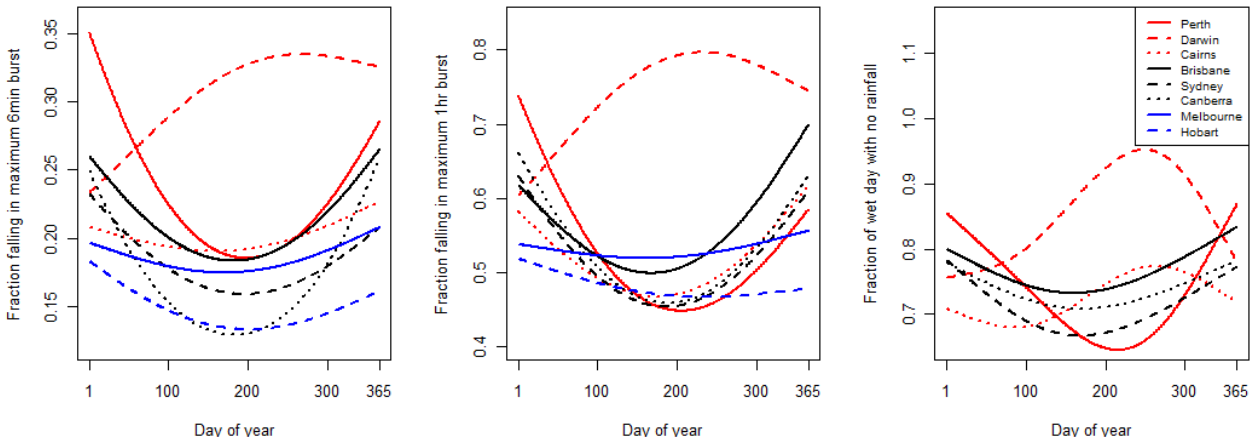

Figure 4: Variability of fraction of daily rain falling in maximum 6-minute (left panel) and 1-hour (middle panel), and fraction of day with no rainfall (right panel), against the day of the year. Only stations which had a statistically significant seasonal cycle were presented.

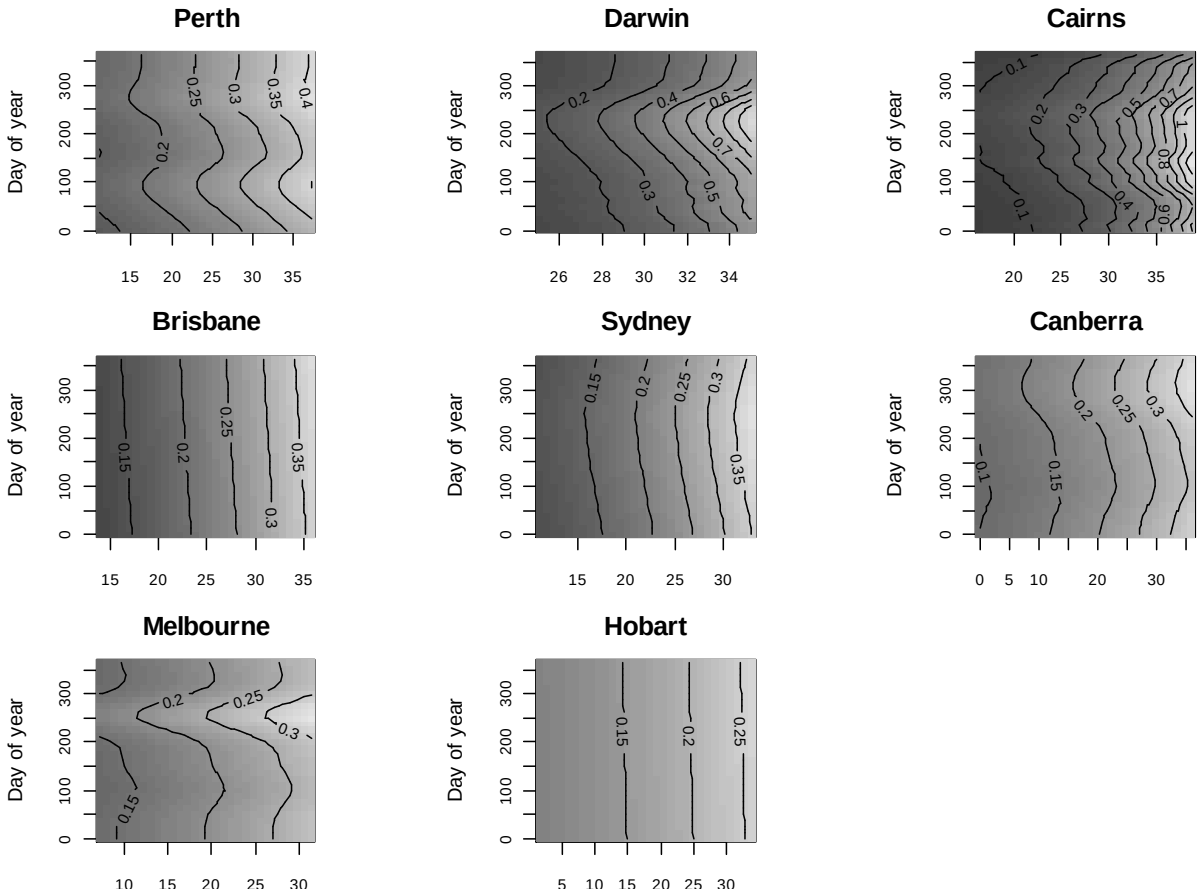

Figure 5: Contour plot of fraction of rain falling as maximum 6 minute storm burst, against maximum 2m daily temperature (x axis) and day of year (y axis).

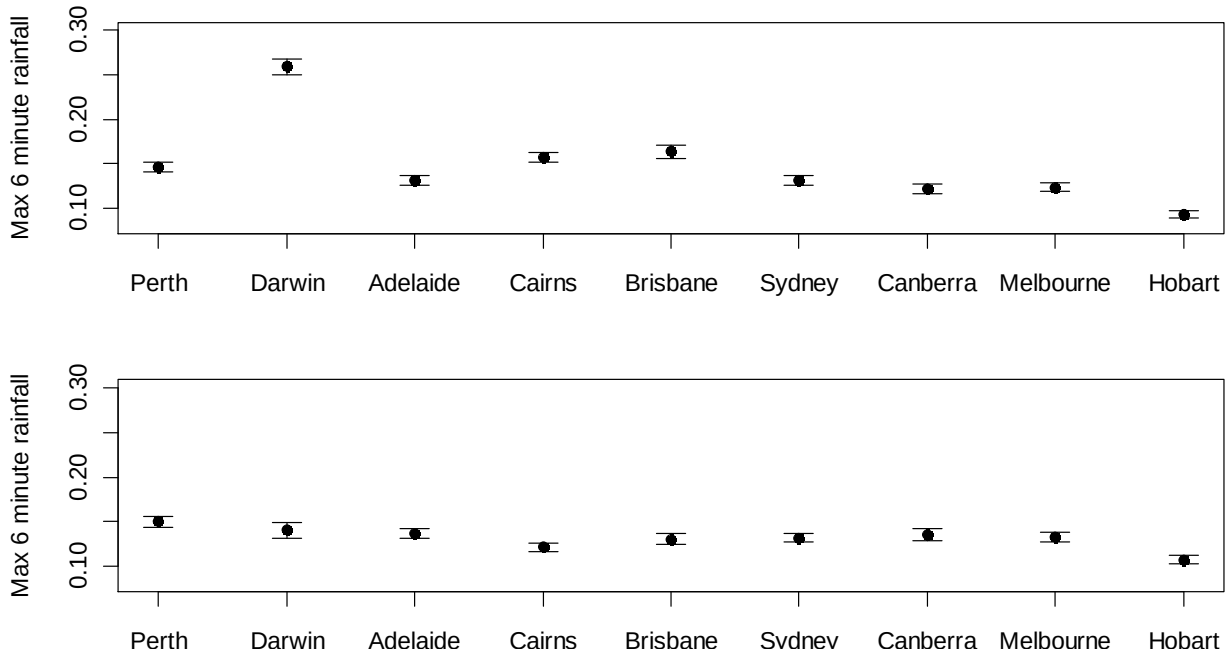

Figure 6: Fraction of rain falling in maximum 6 minute storm burst as a function of station, with the atmospheric temperature set at the mean at each station (upper panel) and the mean across all stations (lower panel). In all cases the daily rainfall amount was set at the mean across all stations. The intervals represent ± 2 standard deviations from the fitted model value.

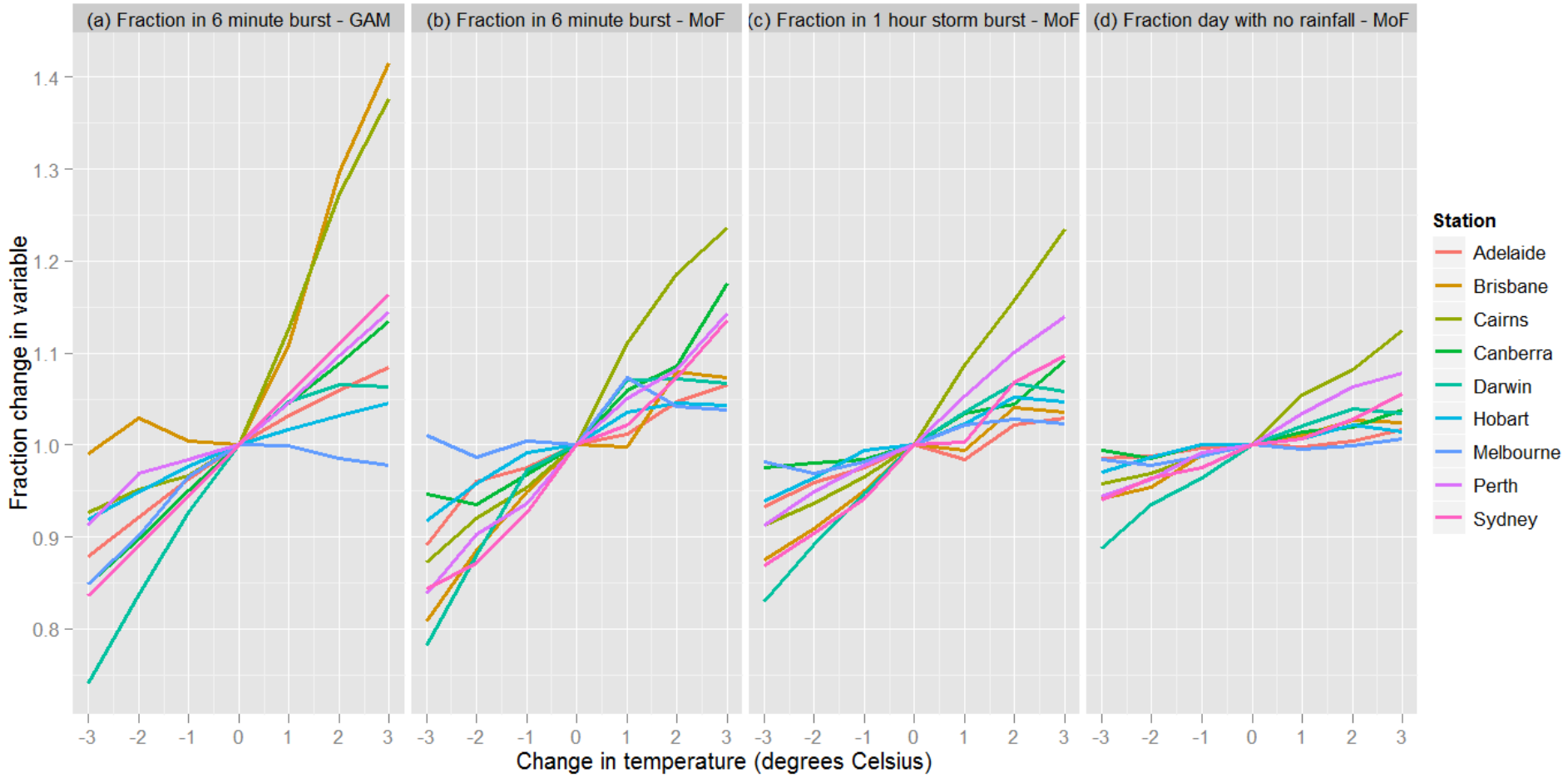

Figure 7: Change in different metrics of daily to sub-daily scaling as a function of changes in atmospheric temperature, simulating directly from the fitted GAM (left panel) or extracted after running the method of fragments approach but conditionally sampling on different atmospheric temperatures. Results using temperature-only covariates.

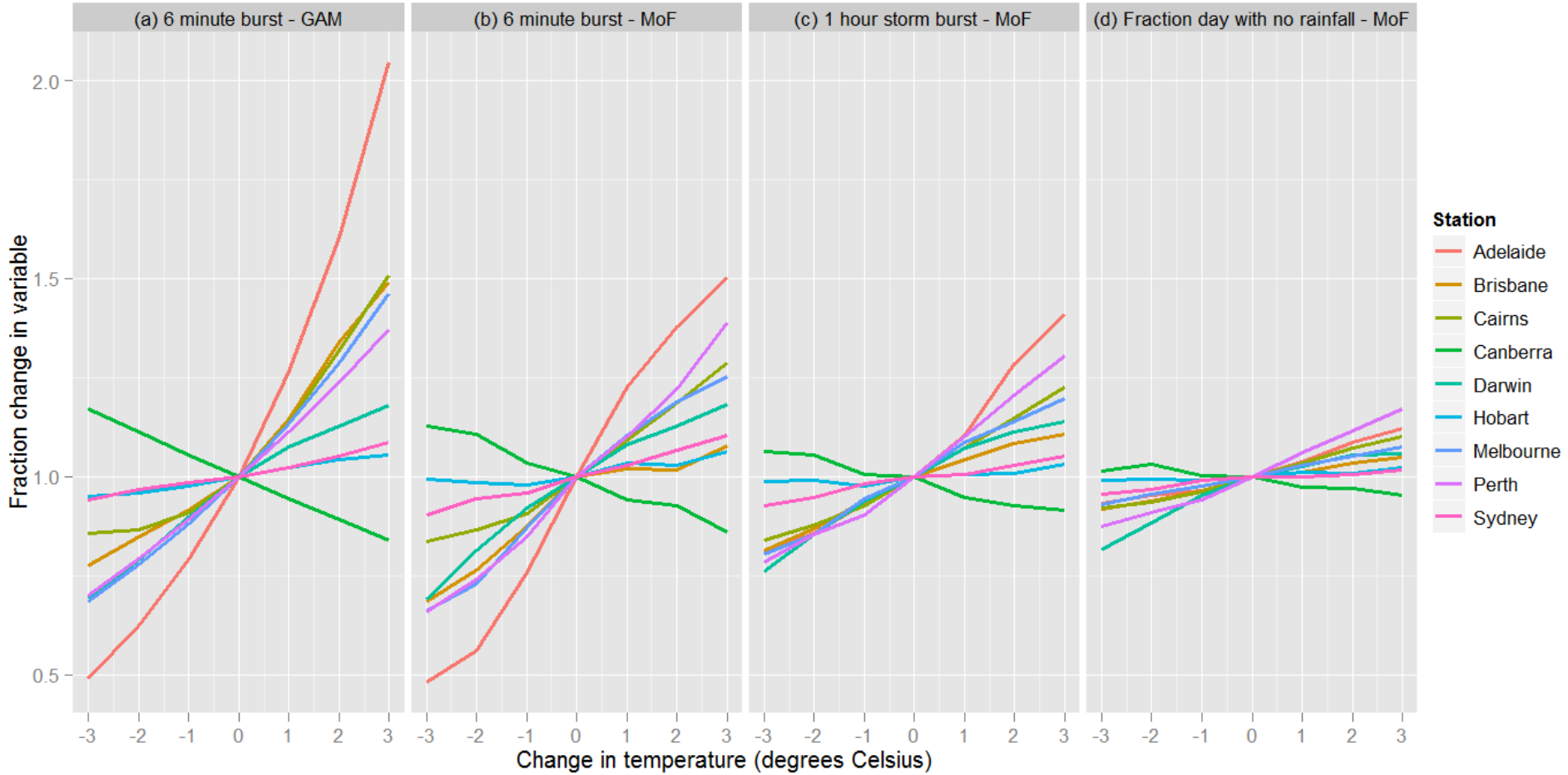

Figure 8: Change in different metrics of daily to sub-daily scaling as a function of changes in atmospheric temperature, simulating directly from the fitted GAM (left panel) or extracted after running the method of fragments approach but conditionally sampling on different atmospheric temperatures. Results using the full set of atmospheric covariates fitted via the mgcv *predictor selection algorithm.*